Title	Validation of coarse grained DEM for simulating loose packing of cohesive powders
Author(s)	Washino, Kimiaki; Faroux, Dorian; Chan, Ei L. et al.
Citation	Advanced Powder Technology. 2025, 36(7), p. 104916
Version Type	VoR
URL	https://hdl.handle.net/11094/102203
rights	This article is licensed under a Creative Commons Attribution 4.0 International License.
Note	

Validation of coarse grained DEM for simulating loose packing of cohesive powders

Kimiaki Washino [a,b,*], Dorian Faroux [a,b], Ei L. Chan [a,b], Tomoya Wakamatsu [b], Takuya Tsuji [a,b], Tatsuya Takahashi [c], Shuji Sasabe [c]

[a] Department of Mechanical Engineering, The University of Osaka, Suita, Osaka 565-0871, Japan
[b] DENSE Ltd., Osaka Kita-ku, Osaka 530-0001, Japan
[c] Hosokawa Micron Corporation, Hirakata, Osaka 573-1132, Japan

ABSTRACT

Coarse grain models for Discrete Element Method (DEM) have been attracting significant attention due to their potential to drastically reduce computational costs. However, their applicability in simulating loose packing behaviour of fine and cohesive powders remains unexplored. The purpose of this study is to validate the Scaled-Up Particle (SUP) model, which is a novel coarse grain model proposed in the authors' previous work, for simulating loose packing behaviour of original cohesive powders. Two distinct particle insertion methods are employed to control the cluster configurations during free fall: random generation of individual particles with initial vertical velocity fluctuations and direct insertion of pre-formed particle clusters. The results show that the final packing structure are strongly influenced by the falling cluster configurations and the SUP model can reproduce a wide range of packing fractions tested in the original cubic particles, from 0.1 for highly cohesive particles to 0.8 for completely cohesionless particles. This highlights the importance of considering collective states of particles to understand bulk powder behaviour.

© 2025 Published by Elsevier B.V. on behalf of The Society of Powder Technology Japan. This is an open access article under the CC BY license (http://creativecommons.org/licenses/by/4.0/).

1. Introduction

Packing of powders is of paramount importance in various processes in industry, and accurate prediction and control of powder packing has been extensively studied [1–3]. Packing fraction or bulk density is the simplest and most accessible macroscopic parameter for evaluating the packing state [4], which can be influenced by the size and other microscopic properties of constituting particles. For fine powders where the particle size is below 100 μm, inter-particle attraction forces such as surface adhesion and van der Waals forces become more dominant than the gravitational force [5], leading to a porous bed structure [6] with low packing fraction. For example, the aluminium sulphate particles used in the authors' previous work [7] gives the packing fraction of 0.25 where the particles are almost cubic in shape with an edge length of approximately 3 μm. While several empirical and semi-empirical expressions exist in the literature for predicting packing fraction [6,8], the correlation between attraction forces, particle properties and the resulting packing state remains largely elusive.

Discrete Element Method (DEM) [9] has been broadly used for simulating various particulate processes. It is a Lagrangian model and directly calculates particle interactions using their microscopic properties to determine the overall flow field. This makes it an ideal tool for studying the packing behaviour of particles [10–15]. However, one of the major drawbacks of DEM is its computational cost. When measuring packing fraction in experiment, a moderate size cup or vessel (at least several centimetres in diameter and height) is filled with particles. Simulating the same process with fine particles using DEM is computationally challenging due to (i) the immense number of particles to be tracked and (ii) the extremely small time steps required to ensure simulation stability. Therefore, very small domain sizes (between 10 and 100 times the average particle diameter) are usually employed in the packing simulations reported in the literature, where the system size can be in the order of or below 100 μm. The packing states in such small systems may differ significantly from those observed in large systems in experiment, but it has not been addressed in the existing literature.

To perform experiment-scale simulations, it is necessary to reduce the computational cost in DEM. Various attempts have been made to achieve this; GPU computing [16–18], MPI domain decomposition [19–21], reduced particle stiffness model [22–27]

---

and coarse grain model [28–33]. In coarse grain models, the size of particles used in simulation is artificially increased while keeping the system size the same so that the number of particles is reduced and the time step may be increased. The coarse grain models proposed in the literature may be classified into two categories: parameter scaling and direct force scaling [34]. In the parameter scaling [29,32,35], the DEM input parameters (such as stiffness and restitution coefficient) are scaled from those of the original particles, usually based on some dimensionless numbers, and plugged into the formula of the force models for the coarse grained particles. In the direct force scaling [28,30,36], on the other hand, the forces acting on the original particles are first estimated using the DEM input parameters and variables (such as particle velocity and overlap) of the original particles and then directly scaled for the coarse grained particles. Relatively recently, several studies in the literature showed coarse grained DEM simulation of cohesive/adhesive particles [37–39]. However, to the best of the authors' knowledge, no studies have reported an in-depth discussion of coarse grain models for simulating loose packing of fine powders.

This study is an extension of the authors' previous work [7] and aims to investigate the applicability of the Scaled-Up Particle (SUP) model, which is a novel coarse grain model proposed in the authors' previous work, in predicting loose packing behaviour of original fine powders. Two distinct particle insertion methods are employed to examine the influence of cluster formation during free fall on the packing state: assigning initial velocity fluctuations to individual particles upon generation and direct insertion of preformed particle clusters. Both original and coarse grained particles are simulated, and the resultant packing fractions are compared to discuss the model validity. LIGGGHTS [40] is used for the simulations, which is open-source and fully customisable.

2. Theory

The theories used for DEM and the SUP model have been explained in the authors' previous work in detail [41,42]. They are briefly summarised in this section.

2.1. Governing equations

The governing equations of Particle i interacting with adjacent Particle j is given by:

$$m_i \dot{\boldsymbol{v}}_i = \sum_j \boldsymbol{F}_{Cij} + m_i \boldsymbol{g} \tag{1}$$

$$\dot{\boldsymbol{L}}_i = \sum_j \boldsymbol{M}_{Cij} \tag{2}$$

$$\boldsymbol{L}_i = \boldsymbol{I}_i \boldsymbol{\omega}_i \tag{3}$$

where m is the particle mass, $\boldsymbol{v}$ is the translational velocity, $\boldsymbol{F}_C$ is the adhesive contact force, $\boldsymbol{g}$ is the gravitational force, $\boldsymbol{L}$ is the angular momentum, $\boldsymbol{M}_C$ is the contact torque, $\boldsymbol{I}$ is the tensor of inertia, and $\boldsymbol{\omega}$ is the angular velocity. The contact torque is given as:

$$\boldsymbol{M}_C = \boldsymbol{r} \times \boldsymbol{F}_C \tag{4}$$

where $\boldsymbol{r}$ is the vector running from the centre of particle to the contact point.

2.2. Shape model

The superquadric model is used to implicitly express the particle shape using the following function [43]:

$$f(\boldsymbol{X}) = \left(\left| \frac{X}{a} \right|^{n_2} + \left| \frac{Y}{b} \right|^{n_2} \right)^{n_1/n_2} + \left| \frac{Z}{c} \right|^{n_1} - 1 \tag{5}$$

$$\boldsymbol{X} = (X, Y, Z)^{\mathrm{T}} \tag{6}$$

where $a, b,$ and c are the size parameters in each principal axis, and n_1 and n_2 are the blockiness parameters that control the edge sharpness. $\boldsymbol{X}$ is the position vector (in local reference frame) from the particle centre, and the particle surface is defined as $f(\boldsymbol{X}) = 0$. Details of the contact detection algorithm for the superquadric model are explained in [44].

2.3. JKR model

The Johnson-Kendall-Roberts (JKR) model [45] is employed for the calculation of adhesive contact force, $\boldsymbol{F}_C$. The normal and tangential contact forces are given by:

$$\boldsymbol{F}_{Cn} = -\left(\frac{4E^*}{3r^*} a_c^3 - 4\sqrt{\pi\gamma E^* a_c^3} + \eta_n \boldsymbol{v}_{rel} \cdot \boldsymbol{n} \right) \boldsymbol{n} \tag{7}$$

$$\boldsymbol{F}_{Ct} = -\min[8G^*\sqrt{r^*\delta_n}\delta_t + \eta_t v_s, \mu_s F_N]\boldsymbol{t} \tag{8}$$

where a_c is the contact radius [12], r is the volume equivalent sphere radius [46], E is the Young's modulus, γ is the surface energy density, η is the viscous damping coefficient [47], $\boldsymbol{v}_{rel}$ is the relative velocity, $\boldsymbol{n}$ is the unit normal vector, G is the shear modulus, δ is the particle deformation (overlap), v_s is the magnitude of the relative tangential velocity at the contact surface, μ_s is the coefficient of sliding friction, F_N is the normal load during sliding [48,49], and $\boldsymbol{t}$ is the unit tangent vector. The subscripts $_n$ and $_t$ indicate the normal and tangential directions, respectively, and the superscript * indicates the reduced quantities. a_c is given as the solution of the following equation [12]:

$$a_c^4 - 2r^*\delta_n a_c^2 - \frac{4\pi\gamma r^{*2}}{E^*} a_c + r^{*2}\delta_n^2 = 0 \tag{9}$$

Note that employing the Gaussian curvature radius or the mean curvature radius at the contact point can give more accurate force evaluation. However, it may require an excessively small time step interval for stable calculation. Employing the volume equivalent sphere radius can reasonably approximate the force–displacement curve according to the work by Podlozhnyuk et al. [44] without compromising the computational cost. The damping coefficients in the normal and tangential directions are given by [47]:

$$\eta_n = -2\sqrt{\frac{5}{3}}\beta(m^*E^*)^{1/2}r^{*1/4}\delta_n^{1/4} \tag{10}$$

$$\eta_t = -4\sqrt{\frac{5}{3}}\beta(m^*G^*)^{1/2}r^{*1/4}\delta_n^{1/4} \tag{11}$$

where β is a function of only the restitution coefficient and given by:

$$\beta = \frac{\ln(e)}{\sqrt{\ln^2(e) + \pi^2}} \tag{12}$$

Following many studies in the literature [50,12,23], the model is simplified so that the contact is broken as soon as the normal overlap becomes zero.

In many simulations of fine powder packing in literature, the non-bonded van der Waals force is also considered [10,12]. The authors proved that both the JKR only model and JKR with non-bonded model can provide comparable results as long as the surface energy density is adjusted to give the same total potential

energy between a pair of particles. More detailed discussions on this topic can be found in [7]. Therefore, the non-bonded van der Waals force is not included in this work to minimise the number of parameters required for the simulations.

2.4. SUP model

In this work, systems with original particle size are called "original systems" whereas those with artificially increased particle size are called "scaled-up systems". l is the scale factor and defined as:

$$l = (m_S/m_O)^{1/3} \tag{13}$$

where the subscripts $_O$ and $_S$ indicate the original and scaled-up systems, respectively. Note that, in the direct force scaling approach [34], the input parameters such as the particle density are unchanged when the particle size is increased.

The Scaled-Up Particle (SUP) model is a novel coarse grain model proposed in the authors' previous work [34,51,52,41,53]. First, the original particle variables, e.g., particle velocity and overlap, are evaluated to estimate the contact forces and torques acting on the original particles. The relationships between the original and scaled-up particle variables are summarised in Table 1 [28,52]: the translational and rotational velocities are given to preserve the total kinetic energy, whilst the particle overlap is determined by the geometric similarity. The estimated forces and torques are then scaled up using the following scaling laws, which are derived to ensure that the fluxes of bulk momentum (i.e., bulk stress) and angular momentum within control volumes are equivalent in the original and scaled-up systems [34,51,53]:

$$F_{IS} = l^2 F_{IO} \tag{14}$$

$$F_{BS} = l^3 F_{BO} \tag{15}$$

$$M_{IS} = l^2 M_{IO} \tag{16}$$

where F_I, F_B and M_I represent any inter-particle forces, body forces and inter-particle torques, respectively. In the simulations presented in this study, the adhesive contact forces are scaled with l^2, gravitational forces with l^3 and the contact torques with l^2.

3. Simulation set-up

3.1. Particle properties

Table 2 shows the common properties of the original particles used in this study. The same properties are also used in the authors' previous work [7]. The size and blockiness parameters are set to $a = b = c = L_e/2 = 1.5$ μm and $n_1 = n_2 = 8$, respectively, to express a cubic particle with an edge length of $L_e = 3$ μm as shown in Fig. 1. The particle shape, size and density are determined based on cubic aluminium sulphate particles (Taimei Chemicals, Japan) [7]. Note that the contact parameters such as friction and restitution coefficients are arbitrarily chosen. It is important to note that the focus of this work is to discuss the validity of the SUP model for simulating the packing behaviour of original fine and cohesive particles. Therefore, the objectives can be fulfilled

Table 1
Relationships between original and scaled-up particle variables.

Variable	Relationship
Translational velocity	$v_O = v_S$
Rotational velocity	$\omega_O = l\omega_S$
Particle overlap	$\delta_O = \delta_S/l$

Table 2
Common properties of particles.

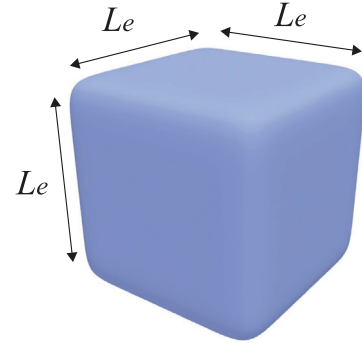| Property	Value
Size parameters $a = b = c$ [μm]	1.5
Blockiness parameters $n_1 = n_2$ [-]	8
Density [kg/m^3]	2730
Young's modulus [MPa]	5
Poisson's ratio [-]	0.3
Coefficient of sliding friction [-]	0.5
Coefficient of restitution [-]	0.3
Surface energy density [J/m^2]	0, 0.00105, 0.0105

Fig. 1. Snapshot of the cubic particle. The edge length of the original particle is $2a = 2b = 2c = L_e = 3$ μm.

as long as the same parameters are used between the original and scaled-up simulations. The friction and restitution coefficients here are within the typical ranges used in the literature, and the parameter sensitivity studies fall outside the scope of this work. Since particle rolling can be largely constrained by the particle shape, the rolling friction model is not used. Three values of surface energy density are employed to vary the cohesiveness of the particles: 0 J/m^2 (cohesionless), 0.00105 J/m^2 (intermediately cohesive) and 0.0105 J/m^2 (highly cohesive). As shown in [7], the particles are cohesive enough although the surface energy densities appear small. This is due to the low Young's modulus used (5 MPa), which results in significant energy dissipation during prolonged particle contact. This effect is thoroughly discussed in the literature [24,27].

3.2. Simulation details

The domain size for the original particle simulations is $60L_e \times 60L_e \times 13333L_e$ as shown in Fig. 2a. Periodic boundary conditions are applied in the horizontal directions, and flat plates are mounted at the top and bottom boundaries. The attraction forces between the top plate and particles are deactivated to prevent particle adhesion. The particles are continuously inserted in the factory region and then settle under the influence of gravity (9.81 m/s^2) to form a stable bed where the packing fraction and bed structure are analysed. The factory region size is $60L_e \times 60L_e \times 267L_e$, and its centre is located at $13133L_e$ in height. It has been proven that the packing fraction can be largely influenced by the formation of particle clusters during free fall [7]. Two distinct particle insertion methods are employed in this work to change the cluster formation. The first method is to randomly generate individual particles with initial vertical velocity fluctuations.

$$v_{init,i} = -v_{ad} + c_{r,i} v_{vf} \tag{17}$$

where $v_{init,i}$ is the initial vertical velocity assigned to Particle i, v_{ad} is the magnitude of average downward velocity, $c_{r,i}$ is the random
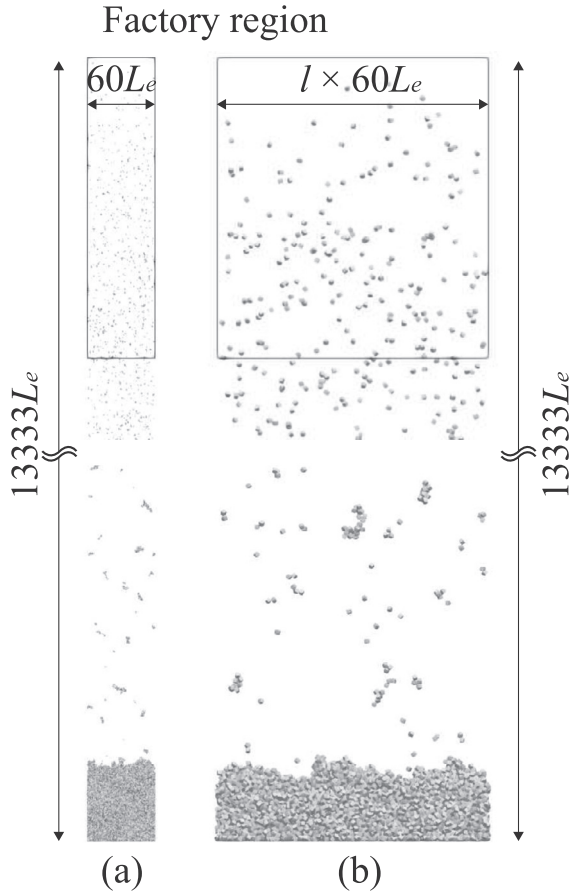
Factory region

Fig. 2. Simulation domain and factory region for the (a) original and (b) scaled-up systems. Periodic boundary conditions are applied in the horizontal directions, and flat plates are mounted at the top and bottom boundaries. The simulation domain is empty before feeding particles.

number between –1 and 1 for Particle i and v_{vf} is the magnitude of vertical velocity fluctuation. The initial horizontal velocity is set to zero, and no overlap is permitted at the generation of the particles. This is called "Insertion Method A" in this work. The second method is to directly insert pre-formed particle clusters with desired configurations. The position of each pre-formed cluster is randomly determined within the factory region. This is called "Insertion Method B".

For the scaled-up simulations, the horizontal dimensions of both the simulation domain and factory region are increased proportionally to the scale factor l to maintain an adequate number of particles for analysis whilst the vertical dimensions are fixed to $13333L_e$ as illustrated in Fig. 2b. The scale factors tested are 1, 2 and 4 where $l = 1$ stands for the original particle. The particle insertion is stopped when the total particle mass reaches $1.2l^2 \times 10^{-8}$ kg.

4. Results and discussion

4.1. Initial velocity fluctuations and cluster configurations

Before performing the packing simulations outlined in Section 3, the relationship between the initial vertical velocity fluctuations and the configuration of particle clusters is first investigated. Particles are generated at once in a simulation box where periodic boundary conditions are applied in all directions including the vertical direction. Gravitational acceleration is set to zero, the overall particle volume fraction is 0.059%, the surface energy density is 0.0105 J/m², v_{ad} is 0 m/s and v_{vf} is varied from 0.1 to 2 m/s.

Fig. 3 shows the average coordination number of particles as a function of dimensionless time, t^*, which is defined as:

$$t^* = \frac{t v_{vf}}{l L_e} \tag{18}$$

where t is the dimensional time. The coordination number here is defined as the number of particles whose bounding spheres are in contact, i.e., the minimal spheres that enclose the cubes. The particles collide and stick with each other, and the cluster size grows with time as indicated by the monotonic increase of the average coordination number. Interestingly, all results in Fig. 3 collapse into almost a single curve, suggesting that similar cluster configurations can be achieved with the SUP model irrespective to the values of the scale factor l and vertical velocity fluctuation v_{vf}. However, it is worth emphasising that the scale factor appears in the denominator of Eq. (18) since the collision density (i.e., the number of collisions per unit volume) decreases with increasing l as reported in the literature [39]. Consequently, larger scaled-up particles experience a slower formation of clusters in terms of the dimensional time. Fig. 4 shows the probability distributions of the particle coordination numbers at $t^* = 100, 3000$ and 50000. It can be observed that not only the average coordination number but the probability distribution at each dimensionless time can be replicated well with the scaled-up particles.

Now, we proceed to reapply the findings above to the context of Insertion Method A in the packing simulation. Since the elevation of the factory region used in the packing simulation is the same regardless of the scale factor as illustrated in Fig. 2, v_{vf} should be scaled with l to give similar configurations of falling clusters before landing. Fig. 5 shows the probability distributions of the particle coordination numbers during free fall when they are continuously inserted in the factory region with $v_{ad} = 0.5$ m/s, $v_{vf} = 0.125l$ m/s and a mass flow rate of $4.02l^2 \times 10^{-8}$ kg/s. The surface energy density used is 0.0105 J/m². The coordination number is analysed for the particles whose centre is located between 0.001 and 0.002 m in height. Fig. 5 proves that almost identical cluster configurations during free fall can be obtained regardless of the scale factor. These results may also imply that the SUP model has a capability of reproducing the dynamics of original particle assemblies, which is an interesting topic for many applications such as granulation and agglomeration. However, it is beyond the scope of the current study and will be discussed in future publications. For now, it suffices to say that we can achieve similar cluster configurations for the onset of the packing simulations by adjusting v_{vf} proportional to the scale factor, which will be used for the simulations presented in Section 4.2.
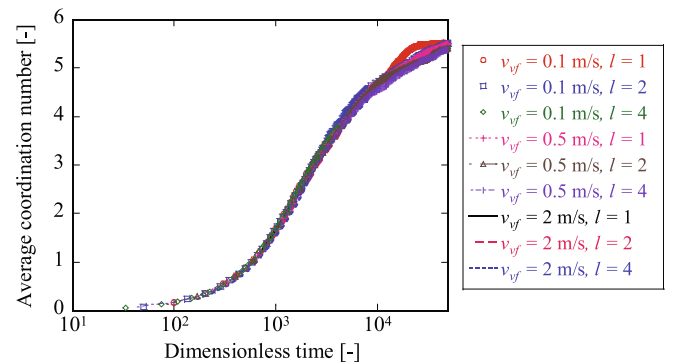

Fig. 3. Average coordination number of particles as a function of dimensionless time $t^* = t v_{vf}/lL_e$ with periodic boundary conditions in all directions. Gravitational acceleration is zero, overall particle volume fraction is 0.059%, surface energy density is 0.0105 J/m² and v_{ad} is 0 m/s.
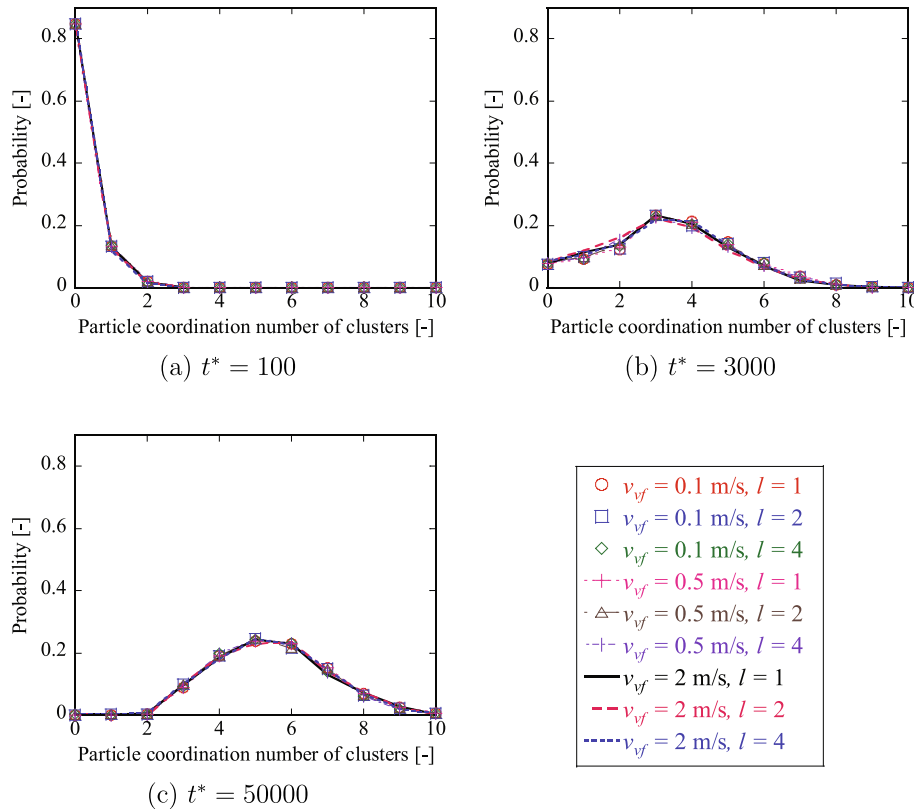
(a) $t^* = 100$

(b) $t^* = 3000$

(c) $t^* = 50000$

○ v_{vf} = 0.1 m/s, l = 1
□ v_{vf} = 0.1 m/s, l = 2
◇ v_{vf} = 0.1 m/s, l = 4
+ v_{vf} = 0.5 m/s, l = 1
△ v_{vf} = 0.5 m/s, l = 2
+ v_{vf} = 0.5 m/s, l = 4
— v_{vf} = 2 m/s, l = 1
- - v_{vf} = 2 m/s, l = 2
···· v_{vf} = 2 m/s, l = 4

Fig. 4. Probability distributions of particle coordination numbers with periodic boundary conditions in all directions. Gravitational acceleration is zero, overall particle volume fraction is 0.059%, surface energy density is 0.0105 J/m² and v_{ad} is 0 m/s.
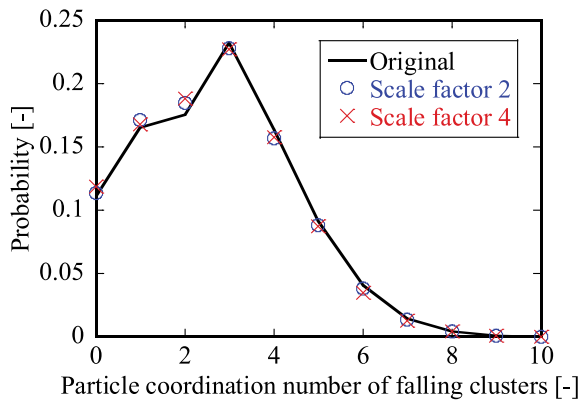
Fig. 5. Probability distributions of particle coordination numbers while falling between the heights of 0.001 and 0.002 m with $v_{ad} = 0.5$ m/s, $v_{vf} = 0.125l$ m/s and mass flow rate of $4.02l^2 \times 10^{-8}$ kg/s. The surface energy density used is 0.0105 J/m².

4.2. Packing simulations with Insertion Method A

In this section, we discuss the results of packing simulations with Insertion Method A. Figs. 6–8 show the profiles of average packing fraction, close-up views of internal particles and the probability distributions of particle coordination numbers within the final beds, respectively, with a surface energy density of 0 J/m² (i.e., cohesionless particles), mass flow rate of $4.02l^2 \times 10^{-8}$ kg/s and v_{ad} of 0.5 m/s. Two values of initial velocity fluctuations are tested: $v_{vf} = 0$ and $0.125l$ m/s. The packing fraction is calculated over sub-domains of size $60lL_e \times 60lL_e \times 2lL_e$ in Fig. 6, and the snapshots above the graphs show the original particles right before landing on the beds. Given the cohesionless nature of the particles

and absence of the clustering during free fall in these snapshots, it is expected that variations in v_{vf} do not have a sensible impact on the resulting packing fraction of the bed. The packing fraction of the bed is approximately 0.8, which is fairly high since cubic particles can align their faces and form an ordered arrangement as observed in Fig. 7, which is also reported in [7]. When computing the probability distributions of particle coordination numbers in the final beds (Fig. 8), only the particles whose vertical position is located between $0.25H_{bed}$ and $0.75H_{bed}$ are included to eliminate the boundary effects where H_{bed} is the height of the final bed. The probability distributions of particle coordination numbers in Fig. 8a and 8b are nearly identical with the peak coordination number at 13.

Figs. 9–11 present the profiles of average packing fraction, close-up views of internal particles and the probability distributions of particle coordination numbers within the final beds, respectively, with a surface energy density of 0.00105 J/m², i.e., intermediately cohesive particles. The bed packing fractions in Fig. 9 are below 0.5, which are considerably lower than the cohesionless cases due to the inter-particle attraction forces. The falling particles form clusters when $v_{vf} = 0.125l$ m/s, whilst the particles lands individually when $v_{vf} = 0$ m/s. However, the formation of falling clusters only gives a marginal decrease of packing fraction in the final bed. This infers that the falling clusters break into fragments because the inter-particle attraction forces are not sufficient to withstand the impact on the bed surface. The ordered structure appeared in the cohesionless cases is no longer observed in Fig. 10, and only limited influence of v_{vf} on the bed structure can be detected in the snapshots. The probability distributions of particle coordination numbers in Fig. 11 exhibit consistent results, and the peak coordination number is much smaller than those of the cohesionless cases. With a closer look at the results, it can be found that
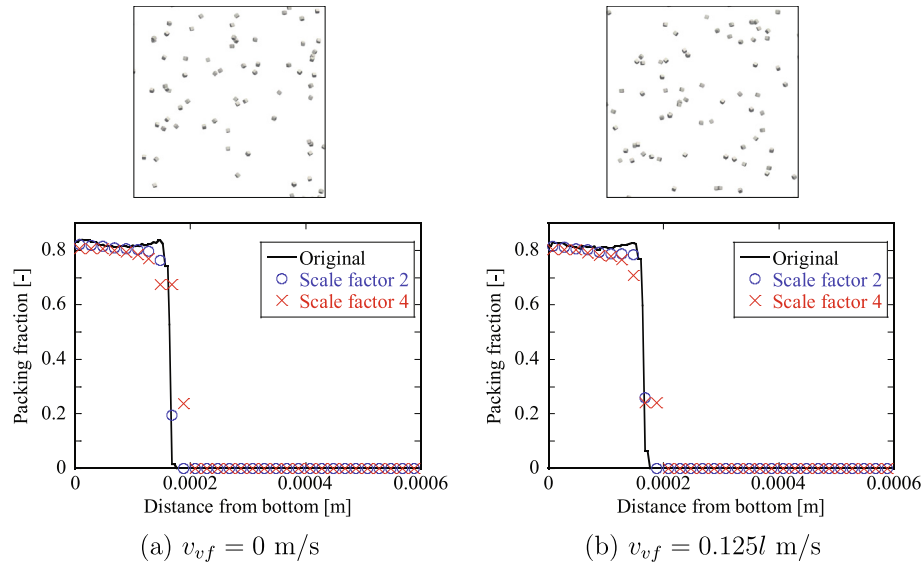
(a) $v_{vf} = 0$ m/s

(b) $v_{vf} = 0.125l$ m/s

Fig. 6. Profiles of average packing fraction of the final beds in the vertical direction from the bottom with a surface energy density of 0 J/m², mass flow rate of $4.02l^2 \times 10^{-8}$ kg/s and v_{ad} of 0.5 m/s. The snapshots above the graphs show the particles right before landing on the beds in the original system.

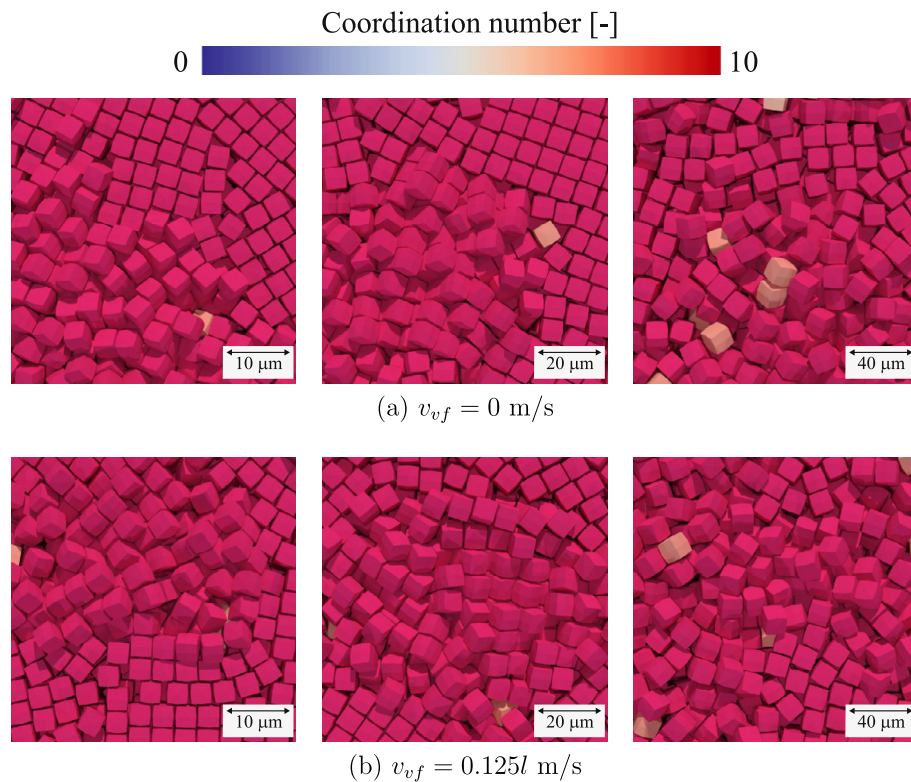(a) $v_{vf} = 0$ m/s

(b) $v_{vf} = 0.125l$ m/s

Fig. 7. Close-up views of internal particles in the final beds with a surface energy density of 0 J/m², mass flow rate of $4.02l^2 \times 10^{-8}$ kg/s and v_{ad} of 0.5 m/s; (left) $l = 1$, (middle) $l = 2$ and (right) $l = 4$.

the peak coordination number shifts slightly but certainly when applying the initial velocity fluctuations: the peak coordination number is 8 when $v_{vf} = 0$ m/s, and is 7 when $v_{vf} = 0.125l$ m/s.

Finally, Figs. 12–14 depict the profiles of average packing fraction, close-up views of internal particles and the probability distributions of particle coordination numbers within the final beds, respectively, with a surface energy density of 0.0105 J/m², i.e., highly cohesive particles. The packing fraction in Fig. 12a

($v_{vf} = 0$ m/s) decreases only slightly from Fig. 9a. When the initial velocity fluctuation is zero, artificially dense packing structure can be formed since all particles land separately on the bed as discussed in [7]. By giving $v_{vf} = 0.125l$ m/s, however, the packing fraction drops significantly and reaches below 0.3 in Fig. 12b. The clusters presented in Fig. 12b are much stronger than those in Fig. 9b, and small inter-cluster voids can be created in the final bed as observed in Fig. 13b. This can be confirmed by the colour
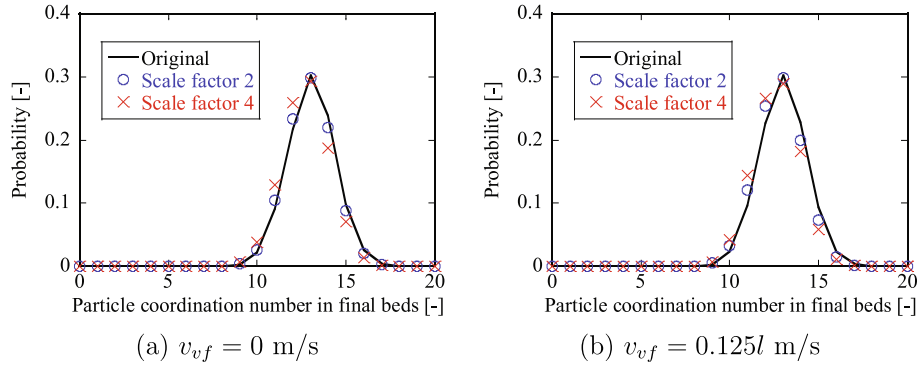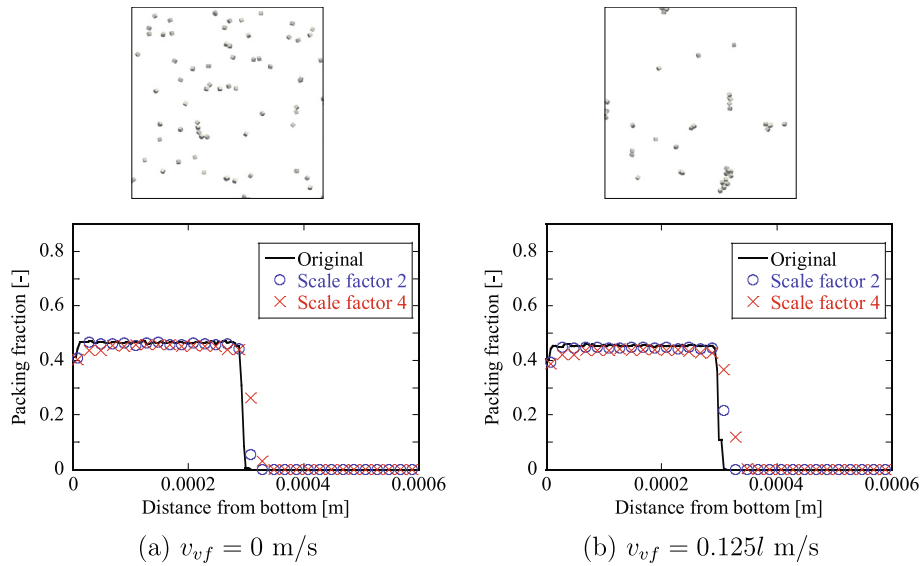
(a) $v_{vf} = 0$ m/s

(b) $v_{vf} = 0.125l$ m/s

Fig. 8. Probability distributions of particle coordination numbers within the final beds with a surface energy density of 0 J/m², mass flow rate of $4.02l^2 \times 10^{-8}$ kg/s and v_{ad} of 0.5 m/s.

(a) $v_{vf} = 0$ m/s

(b) $v_{vf} = 0.125l$ m/s

Fig. 9. Profiles of average packing fraction of the final beds in the vertical direction from the bottom with a surface energy density of 0.00105 J/m², mass flow rate of $4.02l^2 \times 10^{-8}$ kg/s and v_{ad} of 0.5 m/s. The snapshots above the graphs show the particles right before landing on the beds in the original system.

of particles: more light blue particles can be found in Fig. 13b compared to Fig. 13a. Consequently, the peak coordination number in Fig. 14b is smaller than that in Fig. 14a by 2.

Across all results presented in Figs. 6–14, the SUP model can accurately capture the influence of the surface energy densities and initial velocity fluctuations on the resultant packing state. It is interesting that even the slight shift of the peak coordination number by assigning v_{vf} in Fig. 11 can be predicted correctly with the scaled-up particles. The loose packing structures with packing fractions below 0.3 in the original particle beds can be simulated and properly captured using the scaled-up particles, which is, to the best of the authors' knowledge, first proven in this work. One may find these results somewhat counter-intuitive: denser packing structure might be expected with a larger scale factor since the inter-particle attraction force only increases with l^2 whilst the gravitational force increases with l^3 according to Eqs. (14) and (15). For example, consider a scenario where a single original particle is adhering to a fixed wall. As the scale factor increases, the scaled-up particle may detach due to the comparatively weaker attraction force than the gravitational force acting on the particle. However, in the packing simulations above, the bed structure is

determined by the bulk stress, which is exactly what the scaling laws in the SUP model aim to preserve. These results illustrate the importance of considering collective states of particles to understand bulk powder behaviour.

One limitation of Insertion Method A is that it is difficult to obtain consistent cluster configurations when v_{vf} exceeds v_{ad}. As explained in Section 3.2, a plate is placed at the top of the simulation domain, which also coincides with the top of the factory region. When v_{vf} is larger than v_{ad}, some particles possess initial upward velocity, and then they bounce after hitting the top plate. This changes the practical average downward velocity of the particles in the factory region as well as the time taken to reach the particle bed. If the top plate is removed (with an extended simulation domain to contain all particles), some particles are shot upwards and leave the factory region, and the collision frequency deviates significantly from the target value. In either case, the resultant cluster configurations before landing the particle beds are altered undesirably. Therefore, we can only test relatively small v_{vf}, i.e., $0.125l$ in this section so that no particles receive initial upward velocity even with the largest scale factor, where the peak coordination number of the falling particle clusters is 3 (see Fig. 5). The
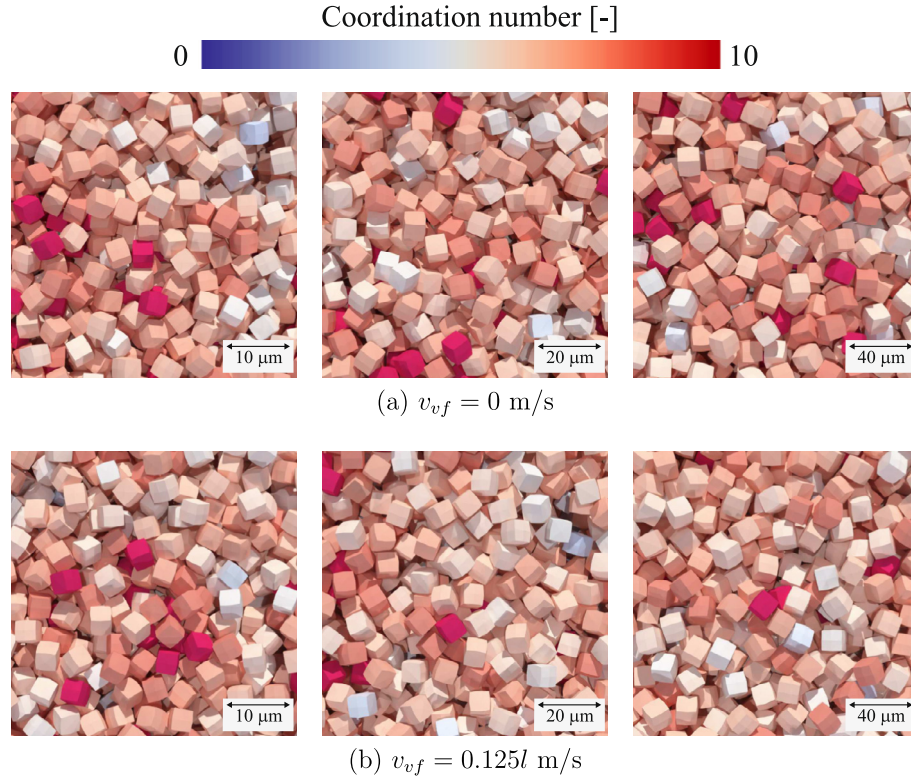
Fig. 10. Close-up views of internal particles in the final beds with a surface energy density of 0.00105 J/m², mass flow rate of $4.02l^2 \times 10^{-8}$ kg/s and v_{ad} of 0.5 m/s; (left) $l = 1$, (middle) $l = 2$ and (right) $l = 4$.
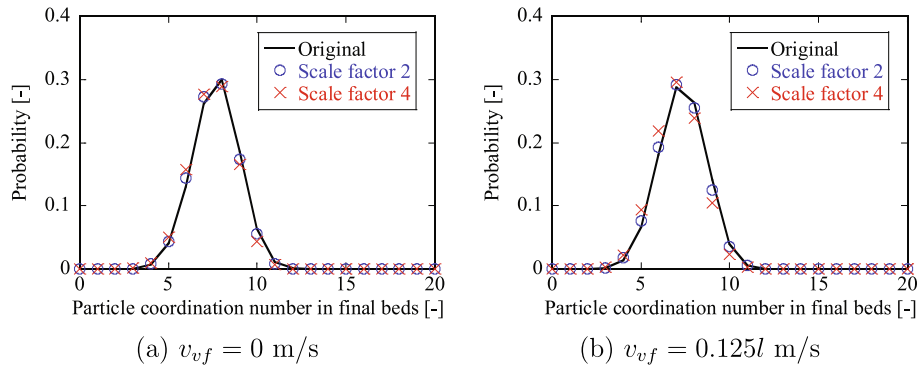

Fig. 11. Probability distributions of particle coordination numbers within final beds with a surface energy density of 0.00105J/m², mass flow rate of $4.02l^2 \times 10^{-8}$ kg/s and v_{ad} of 0.5 m/s.

limitation explained here motivates the use of an alternative method to insert particle clusters with larger coordination numbers, which is the topic of the next section.

4.3. Packing simulations with Insertion Method B

In this section, we discuss the results of packing simulations with Insertion Method B, i.e., direct insertion of pre-formed clusters with desired configurations. The clusters to be inserted here are made of 3000 particles generated within a periodic box of $60L_e \times 60L_e \times 67L_e$ in size, following the same procedure described in Section 4.1. The surface energy density used is 0.0105 J/m², which is the case where the packing results are most sensitive to the falling clusters as demonstrated in Figs. 12–14. A snapshot of the resultant clusters at $t^* = 80000$ as well as the probability distribution of particle coordination numbers are shown in Fig. 15. In

the snapshot, a primary large cluster with tree-like structures can be observed, which is accompanied by smaller satellite clusters. Some of the "branches of the tree" are interconnected and create a large empty space between them. It can be seen that the probability distribution is similar to that shown in Fig. 4c, and the peak particle coordination number is 5. These clusters are inserted continuously with a mass flow rate of $3.34l^2 \times 10^{-7}$ kg/s for the packing simulations. In contrast to Insertion Method A, the initial average velocity and velocity fluctuations are only set to zero to retain the initial cluster structures while falling.

Fig. 16 shows (a) the profiles of average packing fraction in the vertical direction from the bottom and (b) the probability distributions of particle coordination numbers in the final beds. The average packing fraction in Fig. 16a is approximately 0.1, which is much lower than those observed in Fig. 12. It is notable that such a large difference is caused by just increasing the falling cluster
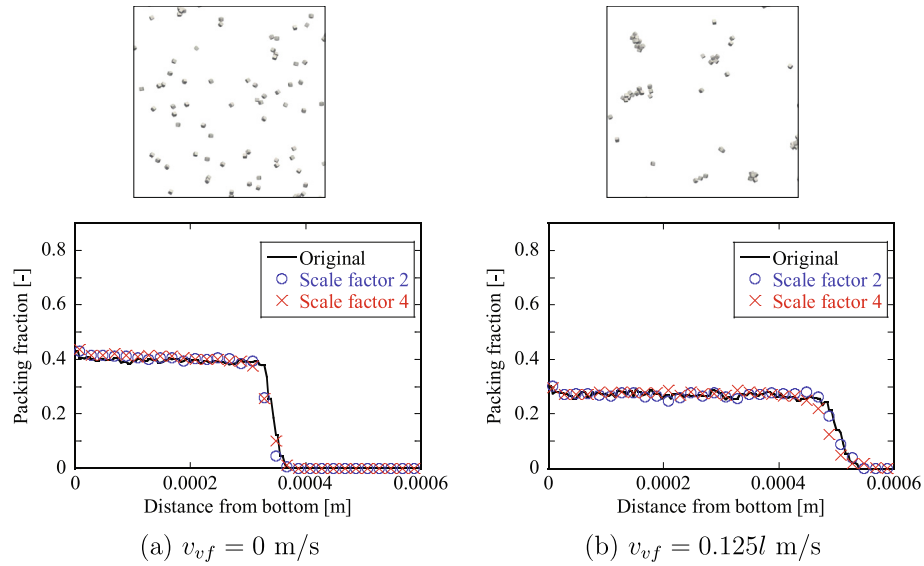
(a) $v_{vf} = 0$ m/s

(b) $v_{vf} = 0.125l$ m/s

Fig. 12. Profiles of average packing fraction of the final beds in the vertical direction from the bottom with a surface energy density of 0.0105 J/m², mass flow rate of $4.02l^2 \times 10^{-8}$ kg/s and v_{ad} of 0.5 m/s. The snapshots above the graphs show the particles above the beds in the original system.

(a) $v_{vf} = 0$ m/s
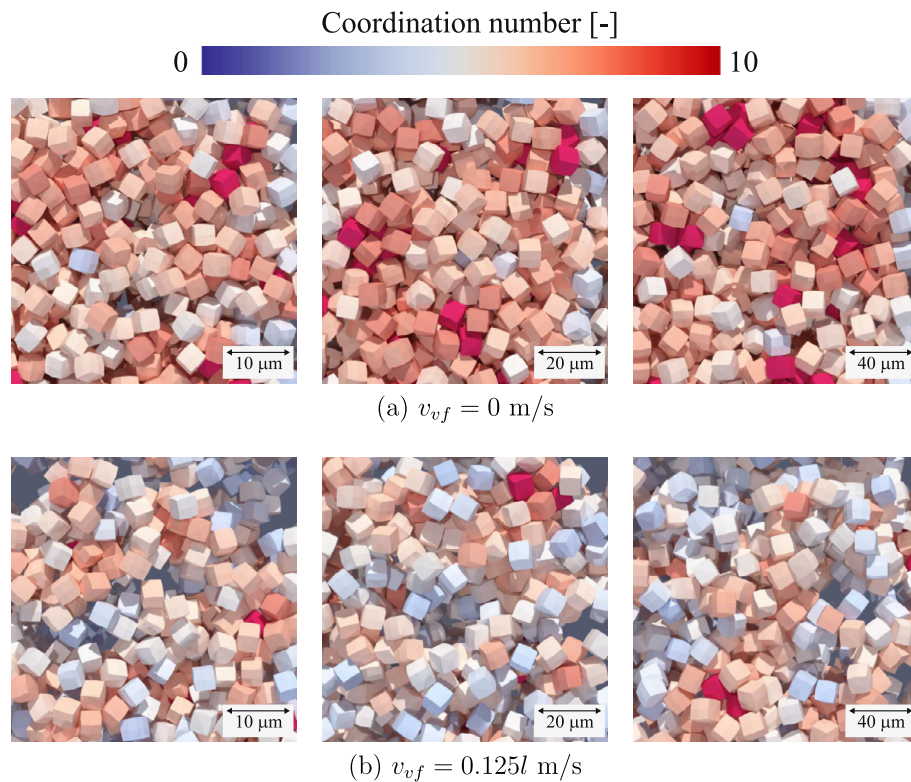

(b) $v_{vf} = 0.125l$ m/s

Fig. 13. Close-up views of internal particles in the final beds with a surface energy density of 0.0105 J/m², mass flow rate of $4.02l^2 \times 10^{-8}$ kg/s and v_{ad} of 0.5 m/s; (left) $l = 1$, (middle) $l = 2$ and (right) $l = 4$.

configurations. In Fig. 16b, the particles with small coordination numbers (below 5) decrease in the final beds as compared with the pre-formed clusters (plotted in the same graph for comparison), whilst those with large coordination numbers (above 5) increase. However, the overall probability distributions between the final beds and pre-formed clusters are similar to a certain extent, implying that the initial cluster structures are partially retained even after landing. Therefore, it is inferred that the low packing fraction of the final beds is caused by large inter-cluster

voids, which can be confirmed in the snapshots in Fig. 17. In the snapshots, very heterogeneous structures can be observed: particles are concentrated in some regions and large voids exist between them. The colour of the particles, which represents the coordination number, is somewhat similar to that in Fig. 15.

It is clear that both the profiles of average packing fraction and probability distributions of coordination numbers in Fig. 16, as well as the snapshots in Fig. 17, obtained from the scaled-up particle simulations are in good agreement with those of the original
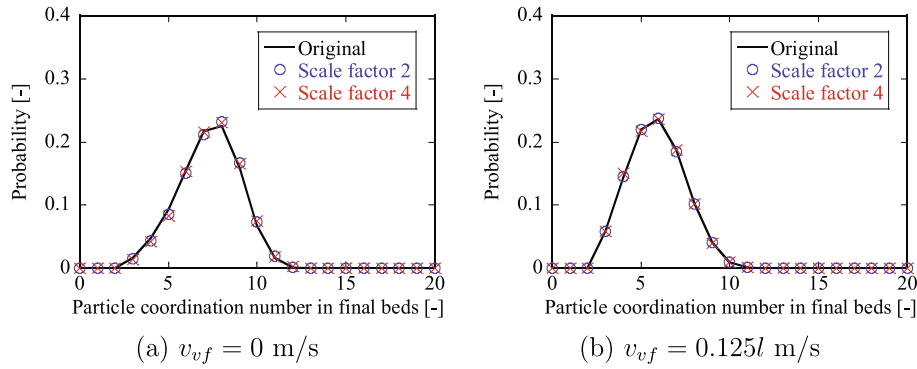
(a) $v_{vf} = 0$ m/s

(b) $v_{vf} = 0.125l$ m/s

Fig. 14. Probability distributions of particle coordination numbers within final beds with a surface energy density of 0.0105 J/m², mass flow rate of $4.02l^2 \times 10^{-8}$ kg/s and v_{ad} of 0.5 m/s.
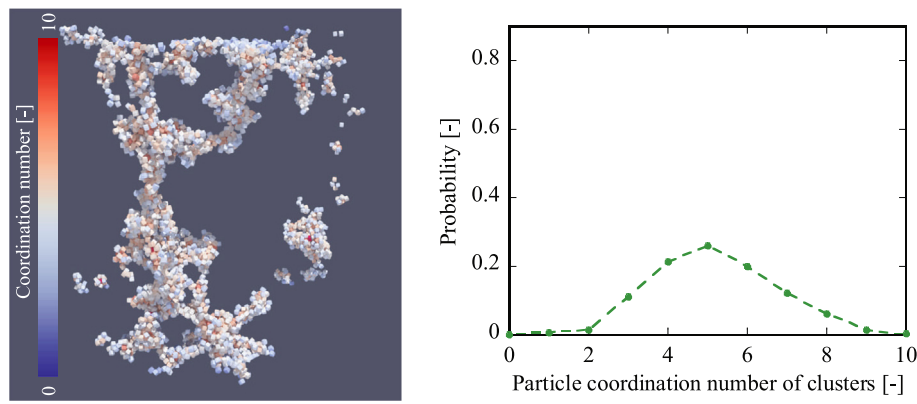

Fig. 15. Pre-formed clusters used for Insertion Method B. The surface energy density used is 0.0105 J/m².
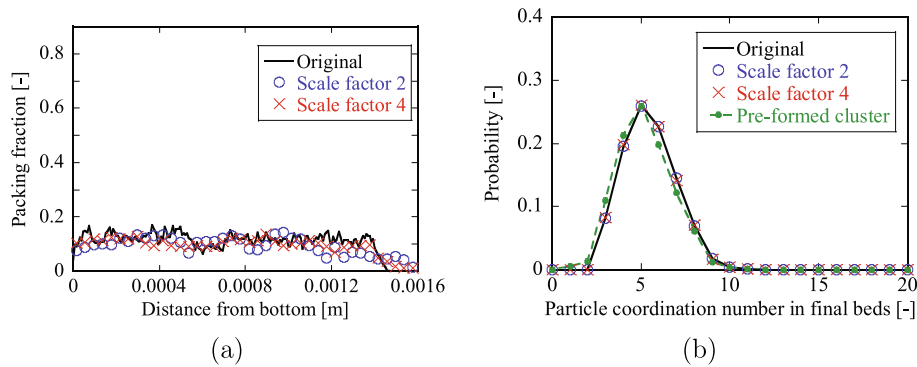

(a)

(b)

Fig. 16. (a) Profiles of average packing fraction in the vertical direction from the bottom and (b) probability distributions of particle coordination numbers of the final beds obtained from Insertion Method B. The surface energy density is 0.0105 J/m² and the mass flow rate is $3.34l^2 \times 10^{-7}$ kg/s.

particle simulation. It is particularly noteworthy that the scaled-up simulations can correctly capture the packing behaviour of the highly complex clusters shown in Fig. 15. These results prove the validity of the SUP model for simulating extremely loose packing behaviour with a packing fraction around 0.1.

5. Conclusions

In this work, the validity of the SUP model, which is a novel coarse grain model for DEM recently proposed by the authors, is discussed for simulating loose packing behaviour of fine and cohesive powders. The adhesive contact force is given by the simplified

JKR model, and particle cohesiveness is controlled by the surface energy density: 0 J/m² for cohesionless, 0.00105 J/m² for intermediately cohesive and 0.0105 J/m² for highly cohesive particles. Original cubic particles with edge length of 3 μm are continuously inserted in a factory region, and the packing fraction and structure of the resulting particle beds are analysed. Two distinct particle insertion methods are employed to examine the influence of cluster formation during free fall on the packing state: random generation of individual particles with initial vertical velocity fluctuations (Insertion Method A) and direct insertion of pre-formed particle clusters with desired configurations (Insertion Method B). Simulations with particle size scale factors of 2 and 4
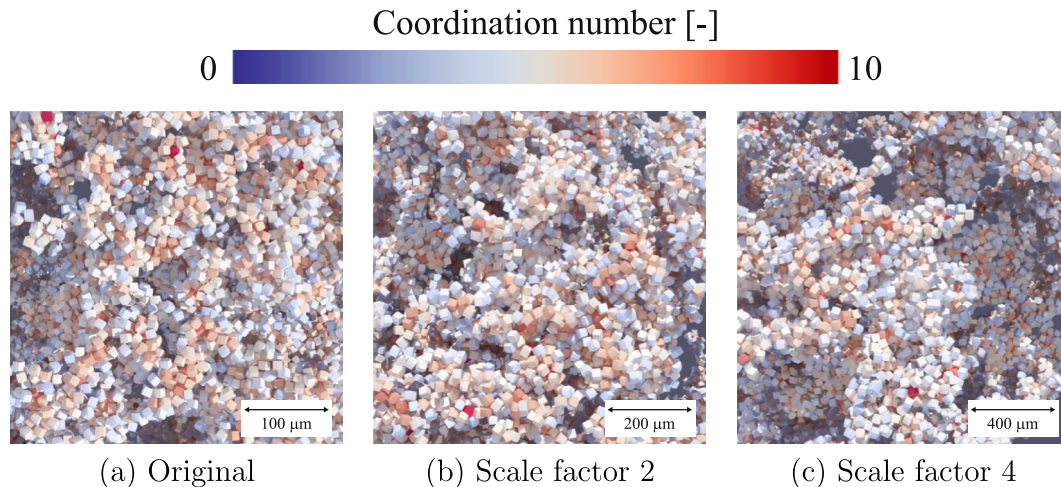
Fig. 17. Close-up views of internal particles in the final beds obtained from Insertion Method B. The surface energy density is 0.0105 J/m^2 and the mass flow rate is $3.34l^2 \times 10^{-7}$ kg/s.

are also performed, and the results are compared with those of the original particles. The key and important results from these simulations are summarised below:

- The coordination numbers of particle clusters coincide when plotted as a function of the dimensionless time defined by Eq. (18). Therefore, with the same elevation of factory regions in both original and scaled-up systems, consistent falling clusters can be achieved simply by scaling the initial velocity fluctuations linearly with the scale factor in Insertion Method A.
- The SUP model accurately predicts the original bed structures of cohesionless, intermediately cohesive and highly cohesive particles for a wide range of packing fractions, including the influence of falling cluster configurations on the resultant packing fraction. This paves the way for an important step torwards large-scale simulations of real-life powders.
- The initial velocity fluctuations should not exceed the average downward velocity in Insertion Method A, which poses a problem when comparing the results with different scale factors.
- Low packing fractions tested, which are below 0.3 with Insertion Method A and approximately 0.1 with Insertion Method B, can be reproduced using the SUP model even though the inter-particle attraction force only increases with l^2 whilst the gravitational force increases with l^3. This is one of the main takeaways of this work, which illustrates the importance of considering collective states of particles to understand bulk powder behaviour, since the SUP model scales the forces and torques to preserve the bulk changes of momentum and angular momentum.

Declaration of Competing Interest

The authors declare that they have no known competing financial interests or personal relationships that could have appeared to influence the work reported in this paper.

Acknowledgements

References

[1] G.D. Scott, Packing of spheres: packing of equal spheres, Nature 188 (1960) 908–909.
[2] Z. Zhang, L. Liu, Y. Yuan, A. Yu, A simulation study of the effects of dynamic variables on the packing of spheres, Powder Technol. 116 (2001) 23–32.
[3] M. Gan, N. Gopinathan, X. Jia, R.A. Williams, Predicting packing characteristics of particles of arbitrary shapes, KONA Powder and Particle Journal 22 (2004) 82–93.
[4] H.P. Zhu, Z.Y. Zhou, R.Y. Yang, A.B. Yu, Discrete particle simulation of particulate systems: a review of major applications and findings, Chem. Eng. Sci. 63 (2008) 5728–5770.
[5] J. Visser, Van der Waals and other cohesive forces affecting powder fluidization, Powder Technol. 58 (1989) 1–10.
[6] A. Yu, J. Bridgwater, A. Burbidge, On the modelling of the packing of fine particles, Powder Technol. 92 (1997) 185–194.
[7] K. Washino, E.L. Chan, D. Faroux, T. Tsuji, T. Takahashi, S. Sasabe, On DEM simulation of loose packing behaviour of fine and cohesive particles, Adv. Powder Technol. 36 (2025) 104809.
[8] G. Roquier, Evaluation of three packing density models on reference particle-size distributions, Granular Matter 26 (2024) 7.
[9] P.A. Cundall, O.D.L. Strack, A discrete numerical model for granular assemblies, Géotechnique 29 (1979) 47–65.
[10] R.Y. Yang, R.P. Zou, A.B. Yu, Computer simulation of the packing of fine particles, Phys. Rev. E 62 (2000) 3900–3908.
[11] S. Yang, K. Dong, R. Zou, A. Yu, J. Guo, Packing of fine particles in an electrical field, Granular Matter 15 (2013) 467–476.
[12] E.J. Parteli, J. Schmidt, C. Blümel, K.E. Wirth, W. Peukert, T. Pöschel, Attractive particle interaction forces and packing density of fine glass powders, Scientific Reports 4 (2014) 1–7.
[13] W. Liu, S. Chen, S. Li, Random loose packings of polydisperse adhesive microparticles with Gaussian size distribution, Powder Technol. 357 (2019) 64–73.
[14] J. Gan, A. Yu, DEM study on the packing density and randomness for packing of ellipsoids, Powder Technol. 361 (2020) 424–434.
[15] A.P. Santos, D.S. Bolintineanu, G.S. Grest, J.B. Lechman, S.J. Plimpton, I. Srivastava, L.E. Silbert, Granular packings with sliding, rolling, and twisting friction, Phys. Rev. E 102 (2020) 032903.
[16] N. Govender, D.N. Wilke, C.Y. Wu, R. Rajamani, J. Khinast, B.J. Glasser, Large-scale GPU based DEM modeling of mixing using irregularly shaped particles, Adv. Powder Technol. 29 (2018) 2476–2490.
[17] Y. He, A.E. Bayly, A. Hassanpour, F. Muller, K. Wu, D. Yang, A GPU-based coupled SPH-DEM method for particle-fluid flow with free surfaces, Powder Technol. 338 (2018) 548–562.
[18] Y. He, F. Muller, A. Hassanpour, A.E. Bayly, A CPU-GPU cross-platform coupled CFD-DEM approach for complex particle-fluid flows, Chem. Eng. Sci. 223 (2020) 115712.
[19] T. Tsuji, K. Yabumoto, T. Tanaka, Spontaneous structures in three-dimensional bubbling gas-fluidized bed by parallel DEM-CFD coupling simulation, Powder Technol. 184 (2008) 132–140.
[20] H. Mio, R. Higuchi, W. Ishimaru, A. Shimosaka, Y. Shirakawa, J. Hidaka, Effect of paddle rotational speed on particle mixing behavior in electrophotographic system by using parallel discrete element method, Adv. Powder Technol. 20 (2009) 406–415.
[21] D. Nishiura, M. Furuichi, H. Sakaguchi, Real-scale DEM simulations on the fault evolution process observed in sandbox experiments, Adv. Powder Technol. 32 (2021) 4432–4441.

[22] T. Kobayashi, T. Tanaka, N. Shimada, T. Kawaguchi, DEM-CFD analysis of fluidization behavior of Geldart Group A particles using a dynamic adhesion force model, Powder Technol. 248 (2013) 143–152.

[23] J. Hærvig, U. Kleinhans, C. Wieland, H. Spliethoff, A. Jensen, K. Sørensen, T. Condra, On the adhesive JKR contact and rolling models for reduced particle stiffness discrete element simulations, Powder Technol. 319 (2017) 472–482.

[24] K. Washino, E.L. Chan, T. Tanaka, DEM with attraction forces using reduced particle stiffness, Powder Technol. 325 (2018) 202–208.

[25] S. Chen, W. Liu, S. Li, A fast adhesive discrete element method for random packings of fine particles, Chem. Eng. Sci. 193 (2019) 336–345.

[26] Y. He, A. Hassanpour, M. Alizadeh Behjani, A.E. Bayly, A novel stiffness scaling methodology for discrete element modelling of cohesive fine powders, Appl. Math. Model. 90 (2021) 817–844.

[27] K. Washino, S. Nakae, R. Yamagami, E.L. Chan, T. Tsuji, T. Tanaka, Scaling of attraction force and rolling resistance in DEM with reduced particle stiffness, Chem. Eng. Res. Des. 203 (2024) 501–519.

[28] M. Sakai, S. Koshizuka, Large-scale discrete element modeling in pneumatic conveying, Chem. Eng. Sci. 64 (2009) 533–539.

[29] C. Bierwisch, T. Kraft, H. Riedel, M. Moseler, Three-dimensional discrete element models for the granular statics and dynamics of powders in cavity filling, J. Mech. Phys. Solids 57 (2009) 10–31.

[30] M. Sakai, H. Takahashi, C.C. Pain, J.P. Latham, J. Xiang, Study on a large-scale discrete element model for fine particles in a fluidized bed, Adv. Powder Technol. 23 (2012) 673–681.

[31] M. Sakai, M. Abe, Y. Shigeto, S. Mizutani, H. Takahashi, A. Viré, J.R. Percival, J. Xiang, C.C. Pain, Verification and validation of a coarse grain model of the DEM in a bubbling fluidized bed, Chem. Eng. J. 244 (2014) 33–43.

[32] S.C. Thakur, J.Y. Ooi, H. Ahmadian, Scaling of discrete element model parameters for cohesionless and cohesive solid, Powder Technol. 293 (2016) 130–137.

[33] A. Di Renzo, E. Napolitano, F. Di Maio, Coarse-Grain DEM Modelling in Fluidized Bed Simulation: A Review, Processes 9 (2021) 279.

[34] E.L. Chan, K. Washino, Coarse grain model for DEM simulation of dense and dynamic particle flow with liquid bridge forces, Chem. Eng. Res. Des. 132 (2018) 1060–1069.

[35] Z. Jiang, K. Rai, T. Tsuji, K. Washino, T. Tanaka, J. Oshitani, Upscaled DEM-CFD model for vibrated fluidized bed based on particle-scale similarities, Adv. Powder Technol. 31 (2020) 4598–4618.

[36] K. Chu, J. Chen, A. Yu, Applicability of a coarse-grained CFD–DEM model on dense medium cyclone, Miner. Eng. 90 (2016) 43–54.

[37] X. Chen, J.A. Elliott, On the scaling law of JKR contact model for coarse-grained cohesive particles, Chem. Eng. Sci. 227 (2020) 115906.

[38] Y. Kosaku, Y. Tsunazawa, C. Tokoro, A coarse grain model with parameter scaling of adhesion forces from liquid bridge forces and JKR theory in the discrete element method, Chem. Eng. Sci. 268 (2023) 118428.

[39] R.S. Larijani, V. Magnanimo, S. Luding, A Coarse-Grained Discrete Element Model (CG-DEM) based on parameter scaling for dense wet granular system, Powder Technol. 453 (2025) 120581.

[40] C. Kloss, C. Goniva, A. Hager, S. Amberger, S. Pirker, Models, algorithms and validation for opensource DEM and CFD-DEM, Progress in Computational Fluid Dynamics, An International Journal 12 (2012) 140.

[41] K. Washino, E.L. Chan, Y. Nishida, T. Tsuji, Coarse grained DEM simulation of non-spherical and poly-dispersed particles using Scaled-Up Particle (SUP) model, Powder Technol. 426 (2023) 118676.

[42] K. Washino, E.L. Chan, T. Tsujimoto, T. Tsuji, T. Tanaka, Development of resolved CFD–DEM coupling model for three-phase flows with non-spherical particles, Chem. Eng. Sci. 267 (2023) 118335.

[43] Barr, Superquadrics and Angle-Preserving Transformations, IEEE Computer Graphics and Applications 1 (1981) 11–23.

[44] A. Podlozhnyuk, S. Pirker, C. Kloss, Efficient implementation of superquadric particles in Discrete Element Method within an open-source framework, Computational Particle Mechanics 4 (2017) 101–118.

[45] K.L. Johnson, K. Kendal, A.D. Roberts, Surface energy and the contact of elastic solids, Proceedings of the Royal Society of London. A. Mathematical and Physical Sciences 324 (1971) 301–313.

[46] G. Pozzetti, B. Peters, A multiscale DEM-VOF method for the simulation of three-phase flows, Int. J. Multiph. Flow 99 (2018) 186–204.

[47] Y. Tsuji, T. Tanaka, T. Ishida, Lagrangian numerical simulation of plug flow of cohesionless particles in a horizontal pipe, Powder Technol. 71 (1992) 239–250.

[48] C. Thornton, Interparticle sliding in the presence of adhesion, J. Phys. D: Appl. Phys. 24 (1991) 1942–1946.

[49] J.S. Marshall, Discrete-element modeling of particulate aerosol flows, J. Comput. Phys. 228 (2009) 1541–1561.

[50] M. Pasha, C. Hare, A. Hassanpour, M. Ghadiri, Analysis of ball indentation on cohesive powder beds using distinct element modelling, Powder Technol. 233 (2013) 80–90.

[51] K. Washino, E.L. Chan, T. Kaji, Y. Matsuno, T. Tanaka, On large scale CFD–DEM simulation for gas–liquid–solid three-phase flows, Particuology 59 (2021) 2–15.

[52] Y. Hu, E.L. Chan, T. Tsuji, T. Tanaka, K. Washino, Geometric similarity on interparticle force evaluation for scaled-up DEM particles, Powder Technol. 404 (2022) 117483.

[53] Y. Hu, E.L. Chan, J.-I. Watanabe, M. Takezawa, T. Tsuji, T. Tanaka, K. Washino, Inter-particle torque scaling in coarse grained DEM with rolling resistance and particle size distributions, Powder Technol. 438 (2024) 119612.